Microcircuit Model of the Dentate Gyrus in Epilepsy

Robert J. Morgan and Ivan Soltesz

Introduction

The dentate gyrus in the mammalian brain is an extremely complex structure containing millions of cells (over 1 million in the rat and many more in primates) of numerous types connected together by billions of synapses. Despite this complexity, the dentate is a highly ordered structure and decades of research have led to a deep understanding of the anatomical and physiological properties of the cells contained therein. Since the dentate is thought to serve as a gate for activity propagation throughout the limbic system (Heinemann et al. 1992; Lothman et al. 1992), understanding of its structure and components is important for developing therapeutic interventions for treating neurological disorders such as epilepsy. Epilepsy and the process by which a normal brain becomes epileptic (epileptogenesis) are complex themselves, however, and result in myriad changes to the dentate gyrus on both molecular and cellular levels. For this reason it is quite difficult to understand the functional implications of specific alterations within the dentate circuitry using traditional methods such as animal models or culture systems. On the other hand, computational models are ideally suited to the task of dissociating the effects of one change from others since it is possible to model only the change of interest. A main drawback of computational modeling is that in order to be confident that what is modeled is an accurate reflection of reality, the model must be sufficiently detailed to reproduce a control situation derived from experimental data. This is especially true for the dentate gyrus as some of the most interesting alterations during epileptogenesis are structural changes that occur on a very large scale and affect the activity and propagation of activity throughout the entire network. Fortunately, the massive amount of experimental data that has been collected about the dentate has facilitated the creation of a large-scale, biophysically realistic computational model that is an excellent tool for studying numerous questions related to how microcircuit changes

R.J. Morgan (✉)
Department of Anatomy and Neurobiology, University of California, Irvine, CA, USA
e-mail: rjmorgan@uci.edu

V. Cutsuridis et al. (eds.), *Hippocampal Microcircuits*, Springer Series in Computational Neuroscience 5, DOI 10.1007/978-1-4419-0996-1_17,

during epileptogenesis affect network activity and propagation of seizures throughout the hippocampus.

In this chapter, we will provide a comprehensive description of a large-scale dentate network model which has evolved from an initial implementation with approximately 500 model cells (Santhakumar et al. 2005) to a network with over 50,000 multicompartmental model neurons (Dyhrfjeld-Johnsen et al. 2007; Morgan and Soltesz 2008). Additionally, we will discuss the experimental data underlying the model parameters and the rationale for the assumptions made in the model. We will then discuss how the model was applied to a problem that is critical for understanding the structure–function relationships of hippocampal microcircuits and highlight the importance of accurate network topology in data-driven models. Finally, we will speculate on potentially useful additions to the dentate model and future questions that could be addressed.

Details of Network Construction

This section will describe the parameters of the dentate gyrus network, including both experimental and model data for comparison (experimental data is derived predominantly from rat, and the model therefore simulates the rat dentate gyrus). The majority of data in this section will be presented in tables in order to provide the reader with a quick and concise way to access a large volume of information.

Construction of a dentate gyrus model requires a number of considerations such as cell types, cell numbers, synaptic connectivity, cellular physiological parameters. These factors can be grouped into two major components which can then be combined to form a complete model. The first component is the connection matrix, which describes as precisely and realistically as possible, the connectivity of each of the cell types in the dentate gyrus. The second component is the model cells themselves, with all of their various properties. This section will present the following in order:

1. Unscaled dentate gyrus connection matrix derived from experimental data
2. Structure of the model cells
3. Passive parameters and channel conductances in the model cells
4. Physiological properties of the cells
5. Scaled model connection matrix with synaptic parameters of model cells

The comprehensive connection matrix of the rat dentate gyrus was constructed from many sources of experimental data, and they are referenced in the appropriate boxes in Table 1. This table contains the eight well-defined cellular subtypes found within the dentate gyrus, their numbers, and their cell type-specific connectivities (for example, from the third row, second column in Table 1: a single basket cell (BC) innervates about 1,250 granule cells (GCs); mean and ranges are indicated). Justifications for the numbers of each cell type as well as the numbers of connections can be found in the following section. While this connection matrix is

Table 1 Connection matrix of the biological dentate gyrus derived from experimental data

	Granule cells	**Mossy cells**	**Basket cells**	**Axo-axonic cells**	**MOPP Cells**	**HIPP cells**	**HICAP cells**	**IS cells**
Granule cells	**X**	**9.5**	**15**	**3**	**X**	**110**	**40**	**20**
(**1,000,000**)	X	7–12	10–20	1–5	X	100–120	30–50	10–30
Ref. [1–5]	Ref. [6]	Ref. [7]	Ref. [6–9]	Ref. [6, 7, 9]	Ref. [6]	Ref. [4, 10, 11]	Ref. [4, 7, 10, 11]	Ref. [7]
Mossy cells	**32,500**	**350**	**7.5**	**7.5**	**5**	**600**	**200**	**X**
(**30,000**)	30,000–35,000	200–500	5–10	5–10	5	600	200	X
Ref. [11]	Ref. [4, 11–13]	Ref. [12, 13]	Ref. [13]	Ref. [13]	Ref. [14]	Ref. [12, 13]	Ref. [12, 13]	Ref. [15]
Basket cells	**1,250**	**75**	**35**	**X**	**X**	**0.5**	**X**	**X**
(**10,000**)	1,000–1,500	50–100	20–50	X	X	0–1	X	X
Ref. [16, 17]	Ref. [4, 16–19]	Ref. [11, 16, 17, 19]	Ref. [16, 17, 20, 21]	Ref. [18]	Ref. [18]	Ref. [18]	Ref. [18]	Ref. [10, 20]
Axo-axonic cells	**3,000**	**150**	**X**	**X**	**X**	**X**	**X**	**X**
(**2,000**)	2,000–4,000	100–200	X	X	X	X	X	X
Ref. [4, 22]	Ref. [4, 18, 22]	Ref. [4, 5, 11, 14, 23]	Ref. [5, 18]	Ref. [5, 18]	Ref. [5, 18]	Ref. [5, 18]	Ref. [5, 18]	Ref. [5, 18, 19]
MOPP cells	**7,500**	**X**	**40**	**1.5**	**7.5**	**X**	**7.5**	**X**
(**4,000**)	5,000–10,000	X	30–50	1–2	5–10	X	5–10	X
Ref. [11, 14]	Ref. [14]	Ref. [14, 24]	Ref. [14, 25]	Ref. [14, 26]	Ref. [14, 25]	Ref. [14, 20, 25]	Ref. [14, 25]	Ref. [14, 15]

Table 1 (continued)

	Granule cells	Mossy cells	Basket cells	Axo-axonic cells	MOPP Cells	HIPP cells	HICAP cells	IS cells
HIPP cells	**1,550**	**35**	**450**	**30**	**15**	**X**	**15**	**X**
(**12,000**)	1,500–1,600	20–50	400–500	20–40	10–20	X	10–20	X
Ref. [11]	Ref. [4, 11, 20]	Ref. [4, 11, 12, 27, 28]	Ref. [4, 11, 20]	Ref. [20, 25]	Ref. [25]	Ref. [14, 20, 25]	Ref. [25]	Ref. [15, 20]
HICAP cells	**700**	**35**	**175**	**X**	**15**	**50**	**50**	**X**
(**3,000**)	700	30–40	150–200	X	10–20	50	50	X
Ref. [5, 29, 30]	Ref. [4, 11, 20]	Ref. [20]	Ref. [4, 11, 20]	Ref. [20]	Ref. [14, 20]	Ref. [20]	Ref. [20]	
IS cells	**X**	**X**	**7.5**	**X**	**X**	**7.5**	**7.5**	**450**
(**3,000**)	X	X	5–10	X	X	5–10	5–10	100–800
Ref. [15, 29, 30]	Ref. [15]	Ref. [15]	Ref. [15, 19]	Ref. [15]	Ref. [19]	Ref. [19]	Ref. [15]	

Cell numbers and connectivity values were estimated from published data for granule cells, mossy cells, basket cells, axo-axonic cells, molecular layer interneurons with axons in perforant-path termination zone (MOPP), hilar interneurons with axons in perforant-path termination zone (HIPP), hilar interneurons with axons in the commissural/associational pathway termination zone (HICAP), and interneuron-selective cells (IS). Connectivity is given as the number of connections to a postsynaptic population (*row 1*) from a single presynaptic neuron (*column 1*). The average number of connections is given in bold. References given correspond to: [1]Gaarskjaer (1978); [2]Boss et al. (1985); [3]West (1990); [4]Patton and McNaughton (1995); [5]Freund and Buzsáki (1996); [6]Buckmaster and Dudek (1999); [7]Acsady et al. (1998); [8]Geiger et al. (1997); [9]Blasco-Ibanez et al. (2000); [10]Gulyas et al. (1992); [11]Buckmaster and Jongen-Relo (1999); [12]Buckmaster et al. (1996); [13]Wenzel et al. (1997); [14]Han et al. (1993); [15]Gulyas et al. (1996); [16]Babb et al. (1988); [17]Woodson et al. (1989); [18]Halasy and Somogyi (1993); [19]Acsady et al. (2000); [20]Sik et al. (1997); [21]Bartos et al. (2001); [22]Li et al. (1992); [23]Ribak et al. (1985); [24]Frotscher et al. (1991); [25]Katona et al. (1999); [26]Soriano et al. (1990); [27]Claiborne et al. (1990); [28]Buckmaster et al. (2002a); [29]Nomura et al. (1997a); [30]Nomura et al. (1997b). Used with permission from Dyhrfjeld-Johnsen et al. (2007).

extremely useful for creating a structural graph of the dentate gyrus (as was done in Dyhrfjeld-Johnsen et al. 2007), and in the future may also be used to create a complete functional model of the dentate, current computing power and experimental data are insufficient to incorporate all of the cell types and cell numbers that are present in vivo into a model containing physiologically realistic cells. Instead, the functional dentate gyrus model is a 1:20 scale model containing four multicompartmental neuronal types: excitatory granule cells and mossy cells, and inhibitory basket cells (BCs) and hilar perforant-path associated (HIPP) cells. The properties of these models cells are depicted in Tables 2, 3, and 4.

Table 2 gives the structural properties of the four cell types implemented in the functional dentate model. Corresponding schematics of these cell types are seen in the top panels of Fig. 1a–d. The passive properties and somatic conductances of these cell types are shown in Table 3, and the physiological properties of the cells are displayed in Table 4. The combination of these two sets of parameters results in biophysically realistic model cells that reproduce the firing properties of cells recorded in vivo. Example traces for each cell type in response to depolarizing and hyperpolarizing pulses are shown in the middle and bottom panels of Fig. 1a–d, respectively.

While Tables 2, 3, and 4 provide a great deal of detail about the single-cell models used to construct the *in silico* dentate gyrus, they do not provide any information about how the cells should be connected together. Using the information in Table 1 as a starting point and accounting for the computational power available to run simulations, a new connection matrix was constructed for the four cell types making up the functional model network. This matrix, along with synaptic parameters for each of the cell type-specific connections, is given in Table 5. Additionally, a schematic diagram illustrating the cell type-specific connectivity of the model is shown in Fig. 2. Note that the dashed line in Fig. 2 that connects the GC to itself represents sprouted GC axon (mossy fiber) connections that do not exist in the healthy dentate gyrus. Rather these connections form as a result of pathological alterations during epileptogenesis, and the number of GC-to-GC connections that exist in the dentate network is a function of the degree of injury to the dentate. This is why GC-to-GC connections are indicated as "Variable" in Table 5. The specific topology of these connections has been shown to play a major role in determining seizure susceptibility in the injured dentate circuit (Morgan and Soltesz 2008) and will be discussed in a later section.

Justification and Explanation of Model Parameters

Cell Types

The following are some of the important factors that determine the cell type:

1. Nature of the neurotransmitter released
2. Location in the laminar structure of the dentate gyrus

Table 2 Structure of model cells

Dimensions	Granule cell	Mossy cell	Basket cell	HIPP cell
Soma				
Diameter, μm	16.8	20	15	10
Length, μm	16.8	20	20	20
Number of dendrites	2	4	4 (2 apical and 2 basal)	4 (2 short and 2 long)
Number of compartments in each dendrite	4	4	4	3
Total number of compartments (soma + dendritic compartments)	9	17	17	13
Dendritic compartments and dimensions			Apical dendrites:	Short dendrites:
Diameter × length, μm	Dendrite in the granule cell layer: 3 × 50	Prox. dendrite: 5.78 × 50	Prox. dendrite: 4 × 75	Prox. dendrite: 3 × 50
	Mid 1 dendrite: 4 × 50	Mid 1 dendrite: 3 × 75	Mid dendrite: 2 × 50	
	Prox. dendrite: 3 × 150	Mid 2 dendrite: 25 × 50	Mid 2 dendrite: 2 × 75	Distal dendrite: 1 × 50
	Mid dendrite: 3 × 150	Distal dendrite: 1 × 50	Distal dendrite: 1 × 75	
	Distal dendrite: 3 × 150			Long dendrites:
			Basal dendrites:	Prox. dendrite: 3 × 75
			Prox. dendrite: 4 × 50	Mid dendrite: 2 × 75
			Mid 1 dendrite: 3 × 50	Distal dendrite: 1 × 75
			Mid 2 dendrite: 2 × 50	
			Distal dendrite: 1 × 50	
References	Aradi and Holmes (1999)	Based on morphological data in Buckmaster et al. (1993)	Based on morphological data in Bartos et al. (2001); Geiger et al. (1997)	Based on morphological data in Buckmaster et al. (2002a); Freund and Buzsáki (1996)

Used with permission from Santhakumar et al. (2005).

Table 3 Passive parameters and maximum conductance of the channels in model cell somata

Mechanism	Source	Granule cell	Mossy cell	Basket cell	HIPP cell
C_m, $\mu F/cm^2$		1	0.6	1.4	1.1
R_a, Ωcm		210	100	100	100
Leak conductance (S/cm^2)	Aradi and Holmes (1999)	0.00004	0.000011	0.00018	0.000036
Sodium (S/cm^2)	Aradi and Soltesz, (2002)	0.12	0.12	0.12	0.2
Delayed rectifier K (Slow) (S/cm^2)	Aradi and Holmes, (1999)	0.006	X	X	X
Delayed rectifier K (Fast) (S/cm^2)	Aradi and Soltesz, (2002)	0.016	0.0005	0.013	0.006
A-type K (S/cm^2)	Aradi and Soltesz, (2002)	0.012	0.00001	0.00015	0.0008
I_h(S/cm^2)	Chen et al. (2001)	X	0.000005	X	0.000015
L-type Calcium (S/cm^2)	Migliore et al. (1995)	0.005	0.0006	0.005	0.0015
N-type Calcium (S/cm^2)	Aradi and Holmes, (1999)	0.002	0.00008	0.0008	X
T-type Calcium (S/cm^2)	Aradi and Holmes, (1999)	0.000037	X	X	X
Ca-dependent K (SK) (S/cm^2)	Aradi and Holmes, (1999)	0.001	0.016	0.000002	0.003
Ca and voltage-dependent K (BK) (S/cm^2)	Migliore et al. (1995)	0.0006	0.0165	0.0002	0.003
Time constant for decay of intracellular Ca (ms)	Aradi and Soltesz, (2002)	10	10	10	10
Steady-state intracellular Ca concentration (mol)	Aradi and Soltesz, (2002)	5×10^{-6}	5×10^{-6}	5×10^{-6}	5×10^{-6}

Used with permission from Santhakumar et al., J Neurophysiol. 2005 Jan;93(1):437–53.

3. Morphological features such as shape of the soma, dendritic arbor, and axonal distribution pattern
4. Presence of specific markers such as calcium binding proteins and neuropeptides

Table 4 Physiological properties of individual cell types

Physiological property	Granule cell		Mossy cell		Basket cell		HIPP cell	
	Model	Biological	Model	Biological	Model	Biological	Model	Biological
RMP (mV)	−70.4	−75 ± 2	−60	−59.7 ± 4.9	−60	−56 to −66	−70	−65 ± 6
R_{in} (MΩ)	183	107–228	210	199 ± 19	64.7	56 ± 9	350	371 ± 47
T_{memb} (ms)	30	31 ± 2	54	24 to 52	8	9–11	17.6	16.9 ± 1.8
AP amp. (mV)	80	86.6 ± 0.7	88	89.8 ± 1.1	78	74 mV	90	83
AP threshold (mV)	−48.70	−49 ± 0.8	−52	−47.33 ± 1.45	−49	−40.5 ± 2.5 (< −52)	−50	−50
Fast AHP (mV)	−7.91	−22.5 to −3.4	−12.2	−15.5	−23.39	−24.9 to −14.9	−18.5	−20 to −7
Spike frequency adaptation	0.31	0.3	0.86	0.8	0.97	.98	0.8	0.82 ± 0.42
Sag ratio	1	0.97 ± 0.01	0.97	0.81 ± 0.02	1	0.9 to 1	0.83	0.78–0.86
Source of biological cell parameters	Lubke et al. (1998); Santhakumar et al. (2000); Staley et al. (1992)		Lubke et al. (1998); Ratzliff et al. (2004); and Santhakumar et al. (2000)		Bartos et al. (2001); Geiger et al. (1997); Harney and Jones (2002); Lubke et al. (1998) and Mott (1997)		Lubke et al. (1998) and Mott (1997)	

Used with permission from Santhakumar et al. (2005).

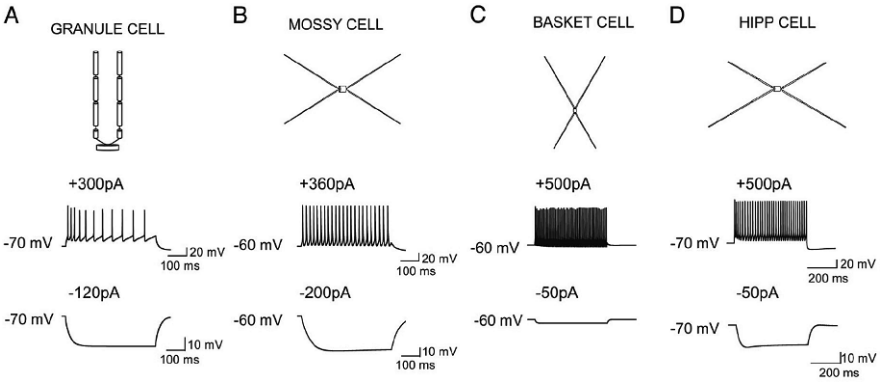

Fig. 1 Structure and intrinsic excitability of model cells. **a**. Schematic representation of the structure (*top*) of the granule cell model and membrane voltage traces of the granule cell in response to 300-pA (*middle*) and 120-pA (*bottom*) current injections. **b**. Illustration of the structure of the model mossy cell (*top*) and the membrane voltage responses to 360-pA (*middle*) and 200-pA (*bottom*) current injections. **c**. The structure of the model basket cell (*top*) and responses to 500 pA (*middle*) and 50 pA (*bottom*) current injections. **d**. Structure (*top*) and responses to 500 pA (*middle*) and 50 pA (*bottom*) of the model hilar perforant-path associated cells (HIPP cells). Used with permission from Santhakumar et al. (2005)

(For detailed description of cell type discrimination see Freund and Buzsáki (1996).) According to the four criteria established above, two excitatory cell types (GCs and MCs) and at least six distinct inhibitory interneurons can be identified in the dentate gyrus (Table 1). Identifying which cell types are appropriate to include in the dentate model is somewhat more complicated than simply identifying the cell types, however. This dilemma occurs because, despite a wealth of information about the dentate gyrus and its cellular composition, there is much information that remains unknown, particularly for the rarer interneuron subtypes. The rationale for including or excluding various cell types from the model based on the available data follows.

Both excitatory cell types (GCs and MCs) are well defined and have a vast amount of electrophysiological data available for the construction of single-cell models. However, the wealth of information available for the interneurons is substantially more limited for many cell types. Additionally, the role of interneurons in the network must be considered with regard to the question being asked. For example, in a model network (such as the one discussed later) that is pursuing the question of the role of topology of sprouted mossy fibers on dentate excitability following injury (Morgan and Soltesz 2008), several factors must be considered. First, the injury to the dentate results in both mossy fiber sprouting and hilar cell loss (including both MCs and inhibitory interneurons). Thus it is critical that the network contains both excitatory cell types plus some form of inhibition. Inhibition can operate in two principal modes. One mode is feed-forward inhibition, where an interneuron is activated by the same afferent input as the excitatory neuron that it contacts. The BC is the primary source of feed-forward inhibition in the dentate gurus (Freund and Buzsáki 1996). The second mode is feedback inhibition, where

Table 5 Functional model network network parameters

From	To -->	GC	MC	BC	HC
Perforant path	Synapse weight (nS)	20	5	10	n/a
	Rise/decay/delay (ms)	1.5/5.5/3	1.5/5.5/3	2/6.3/3	n/a
Granule cells	Convergence	Variable	78.05	370.95	2,266.64
(50,000)	Divergence	Variable	2.34	3.71	27.19
	Synapse weight (nS)	1.00	0.20	0.94	0.10
	Rise/decay/delay (ms)	1.5/5.5/0.8	0.5/6.2/1.5	0.3/0.6/0.8	0.3/0.6/1.5
Mossy cells	Convergence	243.62	87.23	5.59	375.53
(1,500)	Divergence	8,120.82	87.23	1.86	150.21
	Synapse weight (nS)	0.30	0.50	0.30	0.20
	Rise/decay/delay (ms)	1.5/5.5/3	0.45/2.2/2	0.9/3.6/3	0.9/3.6/3
Basket cells	Convergence	3.11	6.31	8.98	n/a
(500)	Divergence	313.22	18.93	8.98	n/a
	Synapse weight (nS)	1.60	1.50	7.60	n/a
	Rise/decay/delay (ms)	0.26/5.5/0.85	0.3/3.3/1.5	0.16/1.8/0.8	n/a
HIPP cells	Convergence	4.82	3.76	140.13	n/a
(600)	Divergence	401.86	9.39	116.77	n/a
	Synapse weight (nS)	0.50	1.00	0.50	n/a
	Rise/decay/delay (ms)	0.5/6/1.6	0.5/6/1	0.4/5.8/1.6	n/a

Used with permission from Dyhrfjeld-Johnsen et al. (2007).

interneurons are activated by excitatory cells which they subsequently inhibit. The BCs and HIPP cells are the two key feedback inhibitory cells in the dentate (Freund and Buzsáki 1996; Buckmaster et al. 2002a). Another important aspect of inhibition is the location of synaptic contact between interneuron and principal cell. Perisomatic inhibition by BCs is considered crucial in maintaining limited GC activity in response to afferent input (limiting the propagation of afferent activity is important for the gating function of the dentate gyrus). The HIPP cells, on the other hand, synapse on the dendritic region near the afferent inputs, and they are likely to modulate integration of dendritic inputs. The loss of this dendritic inhibition with an essentially intact or increased somatic inhibition has been proposed to be particularly relevant to epileptogenesis (Cossart et al. 2001). Furthermore, BCs are resistant to cell death whereas HIPP cells are extremely vulnerable in epileptic tissue (Buckmaster et al. 2002a). These features make the basket and HIPP cells essential constituents of the dentate model.

The remaining four interneurons also possess unique features of inhibition. The molecular layer perforant-path associated (MOPP) cells operate by providing GCs with feed-forward dendritic inhibition (Halasy and Somogyi 1993). The hilar cells with axonal projections to the commissural-associational pathway (HICAP cells) synapse on the proximal dendrites of GCs, near where MC axons terminate and provide feedback inhibition (Freund and Buzsáki 1996). The axo-axonic cells provide GABAergic input at the axon initial segments of GCs and MCs and potentially play powerful roles in modifying spike initiation (Freund and Buzsáki 1996;

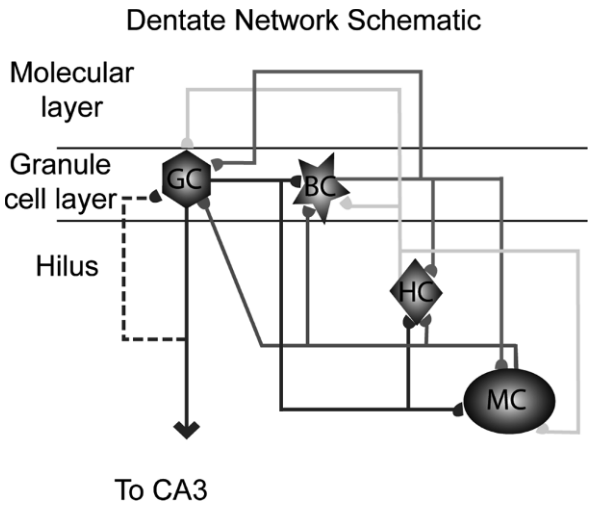

Fig. 2 Schematic of the dentate gyrus model showing the four cell types implemented, the layers in which they reside, and their cell type-specific connectivity. Cell types from left to right: excitatory granule cells (GC, *hexagon*), inhibitory somatically projecting basket cells (BC, *star*), inhibitory dendritically projecting hilar interneurons with axonal projections to the perforant path (HIPP cells, HC, *diamond*), and excitatory mossy cells (MC, *oval*). Dashed line: recurrent GC connections from sprouted mossy fibers following dentate injury. Used with permission from Morgan and Soltesz (2008)

Howard et al. 2005). The interneuron-selective (IS) cells connect exclusively to other interneurons and form a well connected network that could modulate excitability and synchrony of the network.

Unfortunately, detailed physiological data for the development of realistic models of MOPP, HICAP, axo-axonic, and IS cells are not readily available. Therefore, the model of the dentate gyrus presented here contains only basket and HIPP cells as the inhibitory interneurons in the network. Note that the exclusion of other known inhibitory cell types makes it essential to perform control simulations to examine whether augmenting inhibition (in an effort to compensate for excluded cell types) influences the overall outcome of the network simulations. These simulations, among many others aimed at testing the model's robustness, were performed and are thoroughly explained in Dyhrfjeld-Johnsen et al. (2007).

Cell Numbers

Cell numbers can be determined by identifying the cellular layers of the dentate gyrus and then counting the total number of cells in each layer. Then, it is possible to estimate subtype numbers based on the percentage of neurons that express specific markers (Buckmaster et al. 1996; Nomura et al. 1997a, b; Buckmaster et al. 2002a). There are three cell layers in the dentate gyrus: the molecular layer, GC layer, and

hilus (Fig. 2). The GCs are the primary projection cells of the dentate gyrus. These are small, densely packed cells, typically located in the GC layer of the dentate gyrus. The number of GCs in the rat dentate gyrus is approximately 1,000,000 (Gaarskjaer 1978; Boss et al. 1985; West 1990; Patton and McNaughton 1995; Freund and Buzsáki 1996). The other major excitatory cell type, the MC, is located in the hilus and does not express the GABA synthetic enzyme GAD. Buckmaster and Jongen-Relo (1999) estimated the number of GAD-mRNA negative neurons in the dentate hilus (presumed MCs) to be approximately 30,000. The GABAergic interneurons are located in all three layers of the dentate gyrus. These include the BCs, parvalbumin-positive (PV) axo-axonic cells (whose axon terminals project exclusively to the axon initial segment of excitatory cells), somatostatin-positive HIPP cells (Freund and Buzsáki 1996; Katona et al. 1999), nitric oxide synthase-positive HICAP cells (Freund and Buzsáki 1996), and aspiny and calretinin-positive hilar IS cells (Gulyas et al. 1996). The number of GABAergic cell types along the GC-hilar border and in the hilus can be determined based on published histochemical data (Buckmaster et al. 1996; Nomura et al. 1997a, b; Buckmaster et al. 2002a). In the molecular layer, there are approximately 10,000 GAD-mRNA positive interneurons, comprised of approximately 2,000 axo-axonic cells (AACs) (Patton and McNaughton 1995) and 4,000 MOPP cells (Han et al. 1993). The remaining 4,000 cells were excluded from the dentate model, as they are the molecular layer interneurons that project primarily outside of the dentate gyrus such as the outer molecular layer interneurons projecting to the subiculum. Because the HIPP cells are thought to be identical to the somatostatin-positive interneurons in the dentate hilus (Freund and Buzsáki 1996; Katona et al. 1999) and because Buckmaster and Jongen-Relo (1999) estimated that there were 12,000 somatostatin-positive neurons in the hilus, 12,000 HIPP cells were included in the dentate network. HICAP cells are thought to be NOS-positive (Freund and Buzsáki 1996), and because roughly 50% of the nearly 7,000 NOS-positive cells in the hilus are single labeled (i.e., not somatostatin/neuropeptide-Y or calretinin-positive; Nomura et al. 1997a, b), the number of HICAP cells was estimated to be 3,000. The hilus contains about 6,500 calretinin-positive cells (Nomura et al. 1997a, b), roughly 30% of which are somatostatin-positive (presumably spiny calretinin-positive cells), and some calretinin-positive cells overlap with the NOS-positive cells (Nomura et al. 1997a, b). IS cells are aspiny and calretinin-positive (Gulyas et al. 1996), and, assuming that maximally 50% of the calretinin-positive cells are aspiny, we estimated the number of IS cells to be 3,000.

Multicompartmental Single-Cell Models

The single-cell models, as described in Tables 2, 3, and 4, were constructed based on morphological data from the literature (Buckmaster et al. 1993; Freund and Buzsáki 1996; Geiger et al. 1997; Bartos et al. 2001; Buckmaster et al. 2002a). Their intrinsic properties were also modeled based on experimental data, and specific justifications for the passive parameters, ionic conductances, and physiological

properties are described in the following sections. Additionally, the equations used for the single-cell ion channel models are given.

Passive Parameters and Ionic Conductances

The intrinsic properties of the cell types were modeled based on data derived from experiments (Staley et al. 1992; Lubke et al. 1998) that were conducted in the presence of blockers of synaptic activity. The passive membrane parameters and source and densities of active conductances in the somatic compartment of the model cells are listed in Table 3. For GCs, the somato-dendritic distribution of active conductances was adapted from Aradi and Holmes (1999). In all other cell types, the active conductances, with the exception of sodium and fast delayed rectifier potassium channels, were distributed uniformly in all compartments. Sodium and fast delayed rectifier potassium conductances were present only in the soma and proximal dendritic compartments. Additionally, because GCs (Desmond and Levy 1985) and MCs (Amaral 1978) are rich in dendritic spines, the membrane area contribution of dendritic spines was accounted for as in Rall et al. (1992). For GCs, correction for the membrane contribution of spines was performed by decreasing membrane resistivity (increasing leak conductance to $63\,\mu S/cm^2$) and increasing the capacitance to $1.6\,\mu F/cm^2$ (Aradi and Holmes 1999). In the case of MCs (which share several structural and functional properties with CA3 pyramidal cells; Buckmaster et al. 1993), spine density estimates from CA3 cells (Hama et al. 1994) were used to estimate the spine contribution to membrane area. This compensation resulted in an increase of the dendritic leak conductance and capacitance in the MC model.

Physiological Properties

The physiological properties of the model cells were tuned such that the parameters listed in Table 4 were consistent with the data derived from biological cells. The sources for the biological parameters of the various cells are given in Table 4. As is evident from the table, the model cells were accurate replicas of their biological counterparts.

Single-Cell Ion Channel Model Equations

Fast Sodium Current

$$
\begin{aligned}
&I_{\mathrm{Na}} = G_{\mathrm{Na}}(V,t)\cdot(V - E_{\mathrm{Na}}), \quad E_{\mathrm{Na}} = 45\,\mathrm{mV}\\
&G_{\mathrm{Na}}(V,t) = g_{\mathrm{Na}}^{\max}\cdot m^3(V,t)\cdot h(V,t)\\
&\quad \alpha_{\mathrm{m}}(V) = -0.3(V-25)/(e^{(V-25)/-5}-1)
\end{aligned}
$$

$$\beta_{\mathrm{m}}(V) = 0.3(V - 53)/(e^{(V-53)/5} - 1)$$
$$\alpha_{\mathrm{h}}(V) = 0.23/e^{(V-3)/20}$$
$$\beta_{\mathrm{h}}(V) = 3.33/(e^{(V-55.5)/-10} + 1)$$

Fast and Slow Delayed Rectifier Potassium Currents

$$I_{\text{fK-DR}} = G_{\text{fK-DR}}(V,t) \cdot (V - EK), \quad E_{\mathrm{K}} = -85\,\mathrm{mV}$$
$$G_{\text{fK-DR}}(V,t) = g^{\max}_{\text{fK-DR}} \cdot n_f^4(V,t)$$
$$\alpha_{\mathrm{nf}}(V) = -0.07(V - 47)/(e^{(V-47)/-6} - 1)$$
$$\beta_{\mathrm{nf}}(V) = 0.264/e^{(V-22)/40}$$
$$I_{\text{sK-DR}} = G_{\text{sK-DR}}(V,t) \cdot (V - EK), \quad E_{\mathrm{K}} = -85\,\mathrm{mV}$$
$$G_{\text{sK-DR}}(V,t) = g^{\max}_{\text{sK-DR}} \cdot n_s^4(V,t)$$
$$\alpha_{\mathrm{ns}}(V) = -0.028(V - 35)/(e^{(V-35)/-6} - 1)$$
$$\beta_{\mathrm{ns}}(V) = 0.1056/e^{(V-10)/40}$$

A-Type Potassium Current

$$I_{\mathrm{KA}} = G_{\mathrm{KA}}(V,t) \cdot (V - EK), \quad E_{\mathrm{K}} = -85\,\mathrm{mV}$$
$$G_{\mathrm{KA}}(V,t) = g^{\max}_{\mathrm{KA}} \cdot k(V,t) \cdot l(V,t)$$
$$\alpha_{\mathrm{k}}(V) = -0.05(V + 25)/(e^{(V+25)/-15} - 1)$$
$$\beta_{\mathrm{k}}(V) = 0.1(V + 15)/(e^{(V+15)/8} - 1)$$
$$\alpha_{\mathrm{l}}(V) = 0.00015/e^{(V+13)/15}$$
$$\beta_{\mathrm{l}}(V) = 0.06/(e^{(V+68)/-12} + 1)$$

Calcium Channels (T, N, and L-Type)

$$I_{\mathrm{TCa}} = G_{\mathrm{TCa}}(V,t) \cdot (V - E_{\mathrm{Ca}})$$
$$G_{\mathrm{TCa}}(V,t) = g^{\max}_{\mathrm{TCa}} \cdot a^2(V,t) \cdot b(V,t)$$
$$\alpha_{\mathrm{a}}(V) = 0.2(19.26 - V)/(e^{(19.26-V)/10} - 1)$$
$$\beta_{\mathrm{a}}(V) = 0.009e^{-V/22.03}$$
$$\alpha_{\mathrm{b}}(V) = 10^{-6}e^{-V/16.26}$$
$$\beta_{\mathrm{b}}(V) = 1/(e^{(29.79-V)/10} + 1)$$
$$I_{\mathrm{NCa}} = G_{\mathrm{NCa}}(V,t) \cdot (V - E_{\mathrm{Ca}})$$
$$G_{\mathrm{NCa}}(V,t) = g^{\max}_{\mathrm{NCa}} \cdot c^2(V,t) \cdot d(V,t)$$

$$\alpha_c(V) = 0.19(19.88 - V)/(e^{(19.98-V)/10} - 1)$$
$$\beta_c(V) = 0.046e^{-V/20.73}$$
$$\alpha_d(V) = 1.6 \cdot 10^{-4} e^{-V/48.4}$$
$$\beta_d(V) = 1/(e^{(39-V)/10} + 1)$$
$$I_{LCa} = G_{LCa}(V, t) \cdot (V - E_{Ca})$$
$$G_{LCa}(V, t) = g_{LCa}^{max} \cdot e^2(V, t)$$
$$\alpha_e(V) = 15.69(81.5 - V)/(e^{(81.5-V)/10} - 1)$$
$$\beta_e(V) = 0.29e^{-V/10.86}$$

Calcium-Dependent Potassium Channels (Big K and Small K)

$$I_C = G_{BK}(V, [Ca^{2+}], t) \cdot (V - E_K), \quad E_K = -85\,\text{mV}$$
$$G_{BK}(V, [Ca^{2+}], t) = g_{BK}^{max} \cdot r(V, t) \cdot s^2([Ca^{2+}])$$
$$\alpha_r(V) = 7.5$$
$$\beta_r(V) = 0.11/e^{(V-35)/14.9}$$
$$s_\infty = 1/(1 + 4/[Ca^{2+}])$$
$$\tau_s = 10$$

$$I_{AHP} = G_{SK}([Ca^{2+}]) \cdot (V - E_K), \quad E_K = -85\,\text{mV}$$
$$G_{SK}([Ca^{2+}]) = g_{SK}^{max} \cdot q^2([Ca^{2+}])$$
$$\alpha_q([Ca^{2+}]) = 0.00246/e^{(12 \cdot \log_{10}([Ca^{2+}]) + 28.48/-4.5}$$
$$\beta_q([Ca^{2+}]) = 0.006/e^{(12 \cdot \log_{10}([Ca^{2+}]) + 60.4/35}$$

Hyperpolarization-Activated Current

$$I_h = G_h(V, t) \cdot (V - E_h)$$
$$G_h = g_h^{max} \cdot c^2(V, t)$$
$$c(V) = 1/(1 + e^{(V-V50)/10}), \quad V_{50soma} = -81\,\text{mV};\ V_{50distaldend} = -91\,\text{mV}$$
$$\tau_{fast}(V) = 14.9 + 14.1/(1 + e^{-(V+95.2)/0.5})$$
$$\tau_{slow}(V) = 80 + 172.7/(1 + e^{-(V+59.3)/-0.83})$$

Additional details on single-cell ion channel models can be found in Aradi and Holmes (1999) and Chen et al. (2001).

Network Parameters

Network Scaling

The size of the model network is a critical issue both for biological realism and computational feasibility. For a network that is implemented with the goal to study the effects of network topology on excitability (as this one was), preserving the structure of the biological network as much as possible is extremely important. On the other hand, obtaining meaningful results in a reasonable timeframe is also a priority. This balance can only be reached by scaling the dentate gyrus network to a size in which simulations can be run on an hours-to-days timescale (approximate runtime of the described model ranged from 12 to 24 h per simulation on a Tyan Thunder 2.0 GHz dual Opteron server with 32 GB RAM) while allowing biologically realistic cell type-specific connectivity (as described below) to be implemented between neurons. The dentate network model was therefore created as a 1:20 scale model of the biological dentate. Cell numbers and other network parameters are detailed in Table 5. Cell type-specific connectivity numbers were determined as described below and subsequently scaled down by a factor of 20 for use in the model. The number of connections was then increased by a factor of 5 in order to prevent cells in the network from becoming disconnected. Synaptic weights were scaled down appropriately to compensate for the increased connectivity.

Cell Type-Specific Connectivity

Over many years a vast amount of high quality data about the connectivity of the dentate gyrus has been collected, and from this data arose the cell type-specific connectivity matrix for the dentate gyrus (Table 1). Each value presented in the table was determined by a detailed survey of the anatomical literature and was based on an assumption of uniform bouton density along the axon of the presynaptic cell. This assumption is in agreement with the in vivo data of Sik et al. (1997), and it is extremely useful in modeling because it greatly simplifies the estimation of connectivity from anatomical data on axonal length and synapse density per unit length of axon. The rationale behind the connectivity of each of the cell types is given in the following eight sections. Finally, the spatial constraints of the model and the role of axonal arbors in shaping cell type-specific connectivity is explained in Spatial Constraints and Axonal Distributions.

Granule Cells

Mossy fibers (GC axons) in the healthy rat dentate gyrus are primarily restricted to the hilus (97%), with few collaterals (3%) in the GC layer (Buckmaster and Dudek 1999). In addition to MCs (Acsady et al. 1998), mossy fibers have also been shown to contact BCs (Buckmaster and Schwartzkroin 1994; Geiger et al. 1997) and PV interneurons (Blasco-Ibanez et al. 2000). With a total of 400–500 synaptic

contacts made by a single mossy fiber (Acsady et al. 1998), the 3% of each axon located in the GC layer (Buckmaster and Dudek 1999) is estimated to contact 15 BCs and 3 axo-axonic cells. In the hilus, a single GC forms large, complex mossy fiber boutons that innervate 7–12 MCs (Acsady et al. 1998), while an estimated 100–150 mossy fiber terminals target hilar interneurons with approximately one synapse per postsynaptic interneuron (Acsady et al. 1998). Gulyas et al. (1992) estimated that a single spiny calretinin-positive cell (presumed HIPP cell) is contacted by about 9,000 GCs. With 12,000 HIPP cells and 1,000,000 GCs, each GC can be estimated to contact about 110 HIPP cells and 40 HICAP cells. Additionally, in agreement with the presence of mossy fiber terminals on aspiny calretinin-positive interneurons (Acsady et al. 1998), 15 mossy fibers are expected to synapse onto IS cells. Since mossy fibers avoid the molecular layer (Buckmaster and Dudek 1999) in the healthy dentate gyrus, it is assumed that they do not contact MOPP cells. However, in animal models of temporal lobe epilepsy, sprouted mossy fibers have been shown to contact up to 500 postsynaptic GCs (Buckmaster et al. 2002b).

Mossy Cells

A single filled MC axon has been reported to make 35,000 synapses in the inner molecular layer (Buckmaster et al. 1996; Wenzel et al. 1997). Assuming a single synapse per postsynaptic cell, a single MC is estimated to contact 30,000–35,000 GCs. Of the 2,700 synapses made by a single MC axon in the hilus, about 40% target GABA-negative neurons (Wenzel et al. 1997). As each MC is estimated to make 1–5 synaptic contacts on a single postsynaptic MC (Buckmaster et al. 1996), it is estimated that each MC contacts about 350 other MCs. (This is likely to be a generous estimate since it is based on the assumption that all GAD negative somata in the hilus represent MCs.) The remaining 60% of the hilar MC axons target GABA-positive cells (Buckmaster et al. 1996; Wenzel et al. 1997), with no reports demonstrating MC synapses onto IS cells. Assuming that there is no preferential target selectivity between HIPP and HICAP cells and that each postsynaptic hilar interneuron receives two synaptic contacts from a single MC axon (Buckmaster et al. 1996), each MC is estimated to contact 600 HIPP and 200 HICAP cells. There is very low MC to interneuron connectivity in the inner molecular layer (Wenzel et al. 1997); MCs could contact 5–10 basket and axo-axonic cells and approximately 5 MOPP cells with somata in the inner molecular layer (Han et al. 1993).

Basket Cells

In the CA3 region of the rat hippocampus, each principal cell is contacted by about 200 BCs (Halasy and Somogyi 1993), but a GC in the dentate could be contacted by as few as 30 BCs. Assuming that each of the 1,000,000 GCs is contacted by 115 BCs each making 1–20 synaptic connections (Halasy and Somogyi 1993; Acsady et al. 2000), it can be estimated that each BC contacts about 1,250 GCs. MCs receive 10–15 BC synapses (Acsady et al. 2000), resulting in an estimate of 75 BC to MC synapses per BC. Approximately 1% of the 11,000 synapses made by

a single BC axon in the GC layer are onto other BCs (Sik et al. 1997), with 3–7 synapses per postsynaptic cell (Bartos et al. 2001). Consequently, each BC in the dentate gyrus contacts approximately 35 other BCs. Since hilar and molecular layer interneurons are not a major target of BCs (Halasy and Somogyi 1993), a single BC may contact 0–1 HIPP cells. Similarly, the BC synapses onto axo-axonic cells, HICAP, and MOPP cells are assumed to be negligible. As PV cells preferentially contact other PV cells in the hilus (Acsady et al. 2000), we assume that BCs do not contact calretinin-positive IS cells (Gulyas et al. 1992).

Axo-Axonic Cells

Most synapses made by axo-axonic cell axons are thought to target GC axon initial segments (Halasy and Somogyi 1993). However, a small fraction of axon collaterals also descend into the superficial and deep hilus (Han et al. 1993; Freund and Buzsáki 1996). In neocortex, an axo-axonic cell makes 4–10 synapses on the axon intial segment of a postsynaptic cell (Li et al. 1992). With 22,000,000 estimated axon initial segment synapses in the GC layer (Halasy and Somogyi 1993) and 4 synapses per postsynaptic cell (based on the data from the neocortex from Li et al. 1992), each of the 2,000 axo-axonic cells are estimated to target about 3,000 GCs. MCs receive axo-axonic cell input (Ribak et al. 1985), and with the comparatively small fraction of axons from axo-axonic cells in the hilus (Han et al. 1993; Freund and Buzsáki 1996), it can be estimated that axo-axonic cells target a number of MCs equal to about 5% of their GC targets, which results in approximately 150 MCs. Since axo-axonic cells primarily target the axon initial segment of non-GABAergic cells (Halasy and Somogyi 1993; Freund and Buzsáki 1996), it may be assumed that these cells do not project to interneurons.

HIPP Cells

HIPP cells have been estimated to contact about 1,600 GCs and 450 BCs with 1–5 synapses per postsynaptic cell (Sik et al. 1997). MCs can have one dendrite in the molecular layer (Buckmaster et al. 1996) which can be targeted by HIPP cell axons, whereas GCs have two primary dendrites (Claiborne et al. 1990; Lubke et al. 1998). Since the MC to GC ratio is approximately 1:30, the MC dendrites constitute only about 1/60 of the targets for HIPP cells. Increasing this fraction to about 1/45 to account for the presence of a few HIPP cell contacts on MCs in the hilus (Buckmaster et al. 2002a) results in an estimate that each HIPP cell contacts about 35 MCs. HIPP cell axonal divergence onto HICAP and MOPP cells in the molecular layer can be assumed to be similar to that of somatostatin-positive cells in CA1 (Katona et al. 1999) and estimated to be 15 connections onto each population. The HIPP cell axonal divergence to axo-axonic cells is estimated to be between the divergence to basket and HICAP cells; therefore the HIPP cell axon likely contacts 30 axo-axonic cells.

MOPP Cells

MOPP cells target an estimated 7,500 GCs in the rat dentate gyrus. While MOPP cell axons project in the horizontal axis to a similar extent as HIPP cells, they show considerably less collateralization (Han et al. 1993), resulting in an estimate of half as many synapses onto MOPP and HICAP cells as HIPP cells make. As MOPP cell axons are restricted to the molecular layer (Han et al. 1993) and do not target the basal dendrites of BCs, they are assumed to contact less than 1/10 the number of BCs targeted by HIPP cells. Likewise, MOPP cells with axons restricted to the outer and middle molecular layers (Han et al. 1993) would not target the hilar dendrites of axo-axonic cells (Soriano et al. 1990) or the axo-axonic cells with somata and proximal dendrites in the hilus (Han et al. 1993). It is estimated that MOPP cells only contact 1–2 axo-axonic cells. As the MOPP cell axonal arbors in the molecular layer (Han et al. 1993) do not overlap with major parts of the dendritic arborizations of MCs (Frotscher et al. 1991), HIPP cells (Han et al. 1993; Sik et al. 1997; Katona et al. 1999), or IS cells (Gulyas et al. 1996), the connectivity to these cells is negligible.

HICAP Cells

Sik et al. (1997) estimated that the septo-temporal extent and bouton density of HICAP cell axons is similar to that of the HIPP cell axons, whereas the estimated axonal length of HICAP cells is approximately half of the HIPP cell axonal length. Thus, it is estimated that HICAP cells contact about half the number of GCs contacted by HIPP cells. However, since HICAP cells have an additional 3% of axon collaterals in the hilus (Sik et al. 1997), their number of postsynaptic MCs can be assumed to be the same as that of the HIPP cells. HICAP cells are assumed to contact less than half the number of BCs targeted by HIPP cells (∼175) and a negligible number of axo-axonic cells. With a total of 26,000 synapses from a single HICAP cell axon (Sik et al. 1997), approximately 700 synapses should be present in the hilus. Assuming 2–5 synapses per postsynaptic cell, each HICAP cell could contact 100–300 hilar cells. Each HICAP cell is assumed to target 50 HIPP and HICAP cells, which, along with 35 synapses on MCs, is in the estimated range. Although the total axonal length of HICAP cells is only about half of that of HIPP cells, the number of MOPP cells targeted is assumed to be the same (∼10–20), as the HICAP cell axons primarily project to the inner molecular layer where both cell bodies and proximal dendrites of MOPP cells are located (Han et al. 1993).

IS Cells

IS cells contact an estimated 100–800 other IS cells and 5–10 (presumably CCK positive) BCs (Gulyas et al. 1996). Acsady et al. (2000) suggested that CCK cells would include both BC and HICAP morphologies and that IS cells also project to somatostatin-positive HIPP cells. These data result in an estimate that IS cells project to 5–10 HICAP cells and HIPP cells.

Spatial Constraints and Axonal Distributions

The dentate gyrus was represented as a 6 mm strip (corresponding to the approximate septo-temporal extent of the rat dentate gyrus; West et al. 1978) subdivided into 60-μm bins. Cells were distributed evenly among these bins. In addition to the cell type-specific connection probabilities derived from the average number of projections from the pre- to the postsynaptic neuronal class in the literature (i.e., according to the connectivity matrix shown in Table 5), the probability of connections from one particular cell A to another cell B was also dependent on the extent of the axonal arbor of cell A and the relative distance between cells A and B. Therefore the cell type-specific connection probability was modified by a factor obtained by the normalized Gaussian fits to the experimentally determined axonal distributions of the presynaptic cells (Fig. 3) and the relative positions of the pre- and postsynaptic neurons within the dentate strip. Within these cell type-specific constraints, connections were made probabilistically on a neuron to neuron basis with a uniform synapse density along the axon (in agreement with the in vivo data in Sik et al. (1997)), treating multiple synapses between two cells as a single link and excluding autapses.

Receptor Types and Synapses

Building a model of a dentate network with thousands of biophysically realistic multicompartmental model cells is only a meaningful venture if those cells have a way to talk to one another. They can do so via synaptic contacts, but the precise synaptic mechanisms to be included in the model must be determined, and again what to include depends on the particular goal of the model. For the dentate model with the previously-mentioned goal of determining the role of mossy fiber topology in promoting excitability after injury, the minimal requirement is to incorporate ionotropic glutamatergic AMPA synapses (for excitatory transmission) and $GABA_A$ synapses (for inhibitory transmission). Experiments from both normal and epileptic animals are constantly ongoing, and as the data become available it will be possible to add other receptors such as NMDA and metabotropic receptors. Each addition to the network must be carefully considered, however, as greater complexity necessarily increases the load on the computational resources. Since the basic circuit effects of mossy fiber sprouting and cell loss post-injury can be simulated by including AMPA and $GABA_A$ synapses, these were the only synaptic subtypes included in the dentate model.

Postsynaptic conductances were represented as a sum of two exponentials (Bartos et al. 2001). The peak conductance (g_{max}), rise and decay time constants, and synaptic delays for each network connection were estimated from experimental data (Kneisler and Dingledine 1995; Geiger et al. 1997; Bartos et al. 2001; Santhakumar et al. 2005) and are given in Table 5.

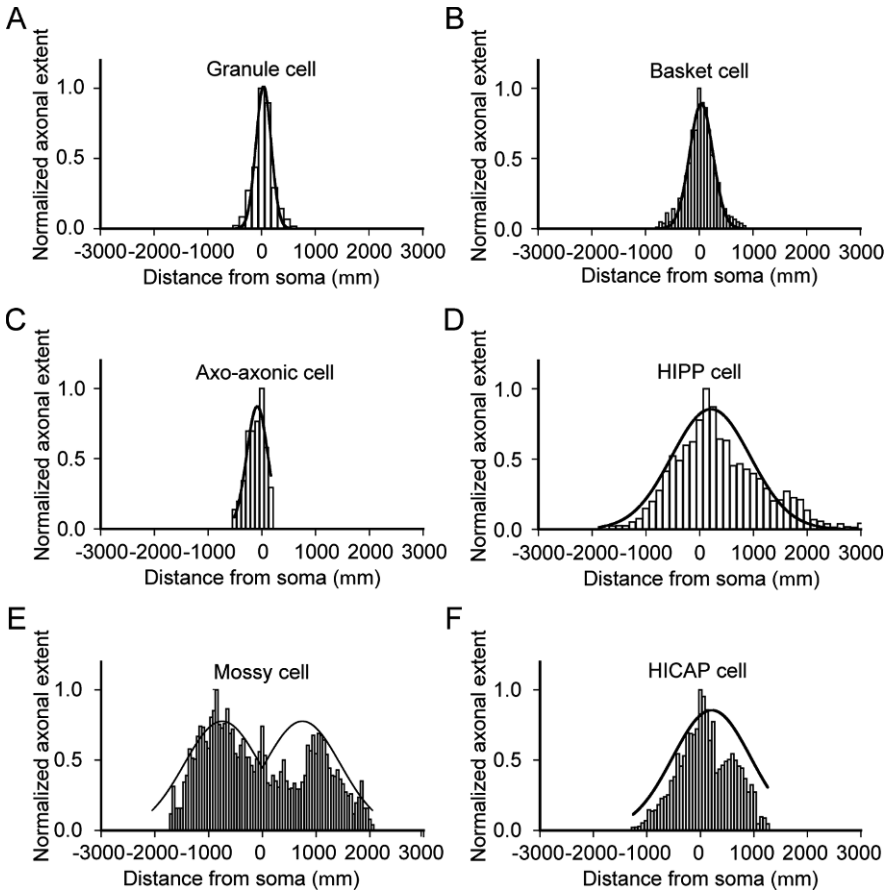

Fig. 3 Gaussian fits to experimentally determined distributions of axonal branch length used in construction of the structural and functional models of the dentate gyrus. **a**. Plot shows the averaged axonal distribution of 13 granule cells (Buckmaster and Dudek 1999) and the corresponding Gaussian fit. **b**. Fit to the septo-temporal distribution of axonal lengths of a filled and reconstructed basket cell (Sik et al. 1997). **c**. Fit to the axonal distribution of a CA1 axo-axonic cell (Li et al. 1992). **d**. Gaussian fit to the averaged axonal distributions of three HIPP cells from gerbil (Buckmaster et al. 2002a). **e**. Fit to averaged axonal distributions of three mossy cells illustrates the characteristic bimodal pattern of distribution (Buckmaster et al. 1996). **f**. Histogram of the axonal lengths of a HICAP cell along the long axis of the dentate gyrus (Sik et al. 1997) and the Gaussian fit to the distribution. All distributions were based on axonal reconstruction of cells filled in vivo. In all plots, the septal end of the dentate gyrus is on the *left* (indicated by negative coordinates) and the soma is located at zero. Used with permission from Dyhrfjeld-Johnsen et al. (2007)

Network Topology

The shape of the network and the way in which connections are made depend strongly on the size of the network. For instance, a network of approximately 50 or 500 cells (Lytton et al. 1998; Santhakumar et al. 2005, respectively) may require

a ring structure to avoid edge effects (i.e., cells on the edge of a network have as few as half as many presynaptic and postsynaptic targets compared to cells in the middle). The network presented here, however, (Dyhrfjeld-Johnsen et al. 2007, Morgan and Soltesz 2008), is large enough that it was set up as a linear strip, more similar to the actual topology of the biological dentate. Similarly, small networks may require non-topographic connectivity. That is, the postsynaptic targets of each cell are selected at random from the pool of potential target neurons while maintaining the cell type-specific divergence and convergence. Larger networks can incorporate the spatial rules discussed above in section "Spatial constraints and axonal distributions" where the connectivity is derived from the axonal distributions and cell type-specific connectivity probabilities established from the literature.

Network topology is an extremely important consideration even on a much finer scale microcircuit level. Indeed, nonrandom connectivity patterns within the recurrent mossy fiber circuit after dentate injury have been shown to play major roles in influencing network excitability (Morgan and Soltesz 2008). The presence of even a small number of highly interconnected GCs that serve as "hubs" can promote seizure-like activity propagation in the dentate. It is therefore very important to carefully consider the potential biological topologies of the network being constructed and, if the particular question the model is designed to answer is thought to be independent of topology, to perform adequate controls to ensure model robustness in the face of topological alterations. The role of network topology in promoting excitability in the dentate microcircuit will be more fully discussed in a later section.

Network Stimulation

The final consideration that must be discussed is the way in which the network is stimulated. The dentate network described in this chapter contains four cell types of which only the MCs have been programmed to have spontaneous activity (and this is a variable parameter which can be turned off by the modeler if desired). Thus, if the network is allowed to run with no afferent stimulus, it will simply sit in a quiescent state with very few neurons firing. This is not entirely uncharacteristic of the dentate gyrus, as it is presumed to be a gate that can filter activity and prevent aberrant propagation throughout the hippocampus, but it is not terribly informative to watch a network do nothing. Additionally, the GCs (among others) in the dentate gyrus are known to receive input from the perforant path (the path that projects from the entorhinal cortex to the hippocampal formation), and this input is quite strong. For this model, the perforant-path input was located on both dendrites of all GCs and the apical dendrites of all BCs. Since 15% of MCs have also been shown to receive direct perforant-path input (Scharfman 1991; Buckmaster et al. 1992), this percentage of MCs also received input. Mass stimulation of the perforant path was simulated by activating a maximum peak AMPA conductance in cells postsynaptic to the stimulation (Santhakumar et al. 2000). The strength of the perforant-path input is shown in Table 5 (note the very large synaptic weight for perforant-path input compared to the small weights for cell-to-cell synapses). In the biological network and in physiological studies it is unlikely that the entire network is activated

simultaneously. Therefore, this network employed a focal stimulation in which a single lamella of the dentate (equivalent to 10% of the dentate strip) was stimulated via the perforant-path input. Other methods of stimulation are also possible, such as providing uncorrelated activation (perforant-path inputs with Poisson distributed interspike intervals; see Dyhrfjeld-Johnsen et al. (2007)) to each GC, BC, and 15% of the MCs. Additional methods for initiation of network activity can be devised as necessary.

Simulated Dentate Injury

Since one of the main purposes of this model was to determine the role of injury-induced structural alterations on network excitability, there had to be a way to simulate the injury. The two primary injury-induced structural alterations in the dentate are the formation of previously nonexistent GC-to-GC connections via mossy fiber sprouting, and the loss of a percentage of MCs and hilar interneurons (the HIPP cells). Mossy fiber sprouting was simulated by first determining the maximum number of new GC-to-GC connections that have been reported in the literature (approximately 275 new connections per GC following pilocarpine-induced status epilepticus in rats (Buckmaster et al. 2002b)), and then scaling this value appropriately (as described for the connectivity above) and implementing the desired percentage of the maximum for moderate injuries. Likewise, hilar interneuron and MC loss were implemented by removing a different percentage of cells at different levels of injury. The model results showed that increasing levels of injury changed both the structure and function of the dentate gyrus, with functional activity closely paralleling the structural alterations. As the dentate network became more highly clustered and interconnected via mossy fiber sprouting, activity increased. However, when nearly all the MCs died, eliminating the primary source of long range connections in the network, the network was no longer as capable of propagating signals over long distances and overall activity and synchrony decreased (Fig. 4, combination of mossy fiber sprouting and cell loss is collectively referred to as "sclerosis" – note that as sclerosis progresses to 80%, there is an increase in network activity followed by a decrease at 100%). The interested reader should refer to Dyhrfjeld-Johnsen et al. (2007) for a more thorough analysis of the topological determinants of epileptogenesis revealed by this model.

Tests for Robustness

As mentioned throughout this chapter, it is important to ensure that the model is robust both in its control state and in its final predictions or in findings to alterations in variables from which the main question should be independent. In a model of this size and complexity, these tests for robustness are particularly important. Therefore, numerous simulations were carried out, and detailed analysis of the various con-

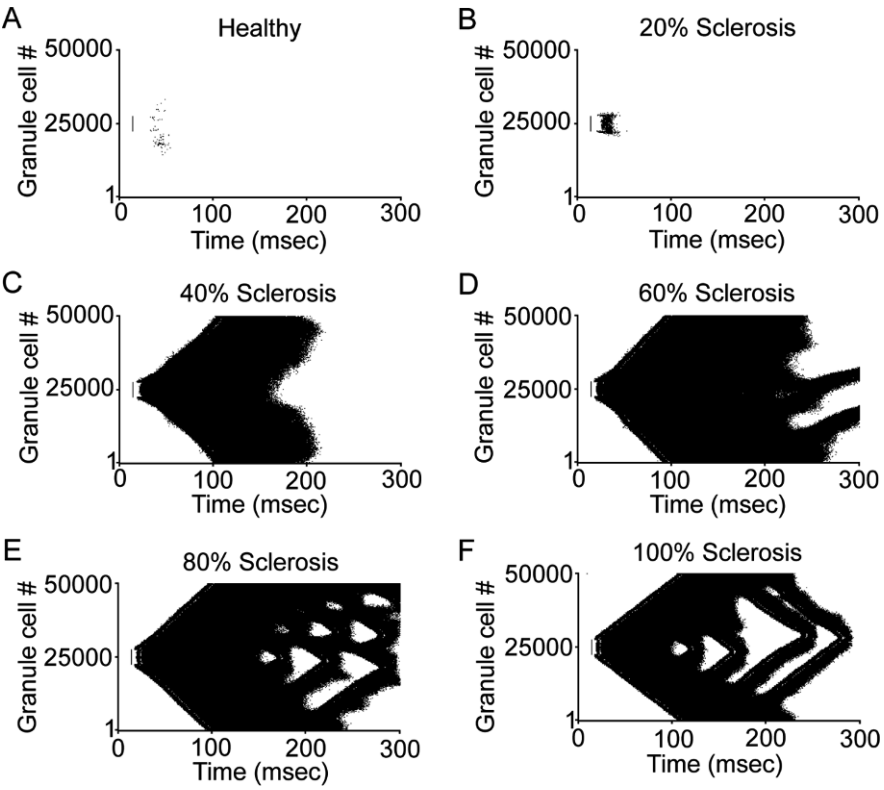

Fig. 4 Effects of the injury-induced topological changes on granule cell activity in functional model networks. **a–f**. Raster plots of the first 300 ms of granule cell action potential firing in the functional model network (Granule cells #1–#50,000, plotted on the y-axis) at increasing degrees of sclerosis. Network activity was initiated by a single stimulation of the perforant-path input to granule cells #22,500 to #27,499 and to 10 mossy cells and 50 basket cells (distributed in the same area as the stimulated granule cells) at t = 5 ms (as in Santhakumar et al. 2005). Note that the most pronounced hyperactivity was observed at submaximal (80%) sclerosis with a decrease in overall activity at 100% sclerosis. Used with permission from Dyhrfjeld-Johnsen et al. (2007)

ditions present in the simulations can be found in Dyhrfjeld-Johnsen et al. (2007). Briefly, the simulations included the following:

1. Variations in cell numbers
2. Variations in connectivity estimates
3. Inhomogeneous distribution of neuron densities along the septo-temporal axis
4. Inhomogeneity in connectivity along the transverse axis
5. Altered neuronal distributions at the septal and temporal poles (the anatomical boundaries of the dentate gyrus)
6. Offset degrees of mossy fiber sprouting and cell loss (after simulated injury)
7. Implementation of a bilateral model of the dentate gyrus including commissural projections and over 100,000 multicompartmental cells

8. Double inhibitory conductance values
9. Variable axonal delays
10. Spontaneous instead of evoked perforant-path stimulation

Using the Dentate Model to Understand the Importance of Hippocampal Microcircuit Topology

The modeling results discussed briefly in section "Simulated Dentate Injury" showed that after dentate injury, the newly formed connections between GCs are instrumental in creating a hyperexcitable dentate network. However, GC-to-GC connectivity is quite sparse; indeed, GCs in the biological dentate only connect to approximately 275 other GCs out of 100,000 potential targets (Buckmaster et al. 2002b). This means that the probability of two GCs connecting, even at maximal levels of sprouting, is only approximately 0.55%, and the probability of random formation of a three-neuron "recurrent" circuit where cell A connects to B which connects to C and back to A is miniscule at 4.16×10^{-6}%. Therefore, the specific patterns of GC-to-GC connections that define the microcircuit structure are likely to play a critical role in affecting network excitability.

The recurrent activity within the GC network may arise from the formation of nonrandom patterns of connectivity that can substantially increase the probability of hyperexcitability and seizures. Other research with this model (such as that described in section "Simulated Dentate Injury") implemented mossy fiber sprouting using random connectivity with the only constraint being the Gaussian distribution of the GC axonal arbors. However, numerous studies have indicated that connectivity in a wide variety of neural systems exhibits highly nonrandom characteristics. For example, the nervous system of the *C. elegans* worm has local connectivity patterns (network motifs) that are over- or underrepresented compared to what would be present in a random network (Milo et al. 2002; Reigl et al. 2004; Sporns and Kotter 2004). These connectivity patterns have dynamical properties that could influence their abundance, closely tying structure to function (Prill et al. 2005). Nonrandom connectivity features such as power-law distributions of connectivity (scale-free topology; Watts and Strogatz 1998; Barabasi and Albert 1999; Dyhrfjeld-Johnsen et al. 2007) and nonrandom distributions of connection strengths (Song et al. 2005) have been discovered in mammalian cortices as well. Additionally, it has been shown that connection probabilities can demonstrate fine-scale specificity that is dependent both upon neuronal type and the presence or absence of other connections in the network (Yoshimura and Callaway 2005).

Morgan and Soltesz (2008) therefore used this model to examine the role of several biologically plausible GC microcircuits on dentate excitability after a moderate insult (resulting in 50% of maximal mossy fiber sprouting and 50% loss of MCs and hilar interneurons). They discovered that a small percentage of highly interconnected GCs serving as network "hubs" can greatly augment hyperexcitability in the model (Fig. 5a, diamonds represent hub cells). This change in hyperexcitability

was mediated only by a change in the topology of GC-to-GC connections in the network (i.e., only the GC-to-GC connections were reconnected such that 5% of all GCs had approximately 5 times as many connections as the average GC; Fig. 5a), as no other network connections were altered and the total number of connections in the dentate network remained constant at all times. Figure 5b displays network activity from this model network incorporating 50% of the maximum mossy fiber sprouting and 50% of MC and hilar interneuron loss when GC-to-GC connections were made randomly. Figure 5c shows activity of the network in which 5% of GCs were vastly more interconnected than the average GC, creating network hubs (Fig. 5a – it was necessary for hubs to have both enhanced incoming as well as outgoing connectivity in order to effectively increase network excitability; refer to Fig. 4d in Morgan and Soltesz (2008)). Figure 5d shows traces from both an average GC and a hub cell, demonstrating the powerful impact that topological changes in hippocampal microcircuits can exert on cellular activity. Inclusion of hub cells massively enhanced excitability of the dentate network without changing the total excitatory drive of the network, demonstrating the importance that hub cells can play seizures.

Computational models are most effectively utilized when they either confirm experimental findings or provide predictions that can be tested experimentally. Therefore, the finding that hub cells can promote hyperexcitability in the dentate means little unless there is biological evidence for the model's prediction. Indeed, there are cells in the dentate gyrus that have a very long basal dendrite which receives many times more incoming excitatory synaptic connections than average GCs (Spigelman et al. 1998). However, these cells with basal dendrites had previously been shown only to have increased incoming connectivity, and the model predicted that hubs need both increased incoming and outgoing connectivity. Until recently, there were no data suggesting whether GCs with basal dendrites form either more numerous or stronger outgoing connections. In agreement with the model, though, a study of post-status epilepticus GCs recently revealed a previously unseen increase in axonal protrusions (often within the GC layer) among newborn cells that likely corresponds to an increased number of outgoing connections onto other GCs (Walter et al. 2007). Additionally, over 40% of post-SE newborn GCs retain a basal dendrite in addition to nearly 10% of mature post-status epilepticus (SE) GCs (Walter et al. 2007), thereby resulting in the probable existence of GCs with both increased axonal protrusions *and* a basal dendrite (i.e., satisfying the model's requirement for both enhanced incoming as well as outgoing connectivity). While more experimental work is necessary to fully characterize the outgoing connectivity of GCs with basal dendrites, our results combined with the described experimental work strongly support the likelihood that neuronal hubs play a hitherto unrecognized, major role in promoting hyperexcitability and seizures.

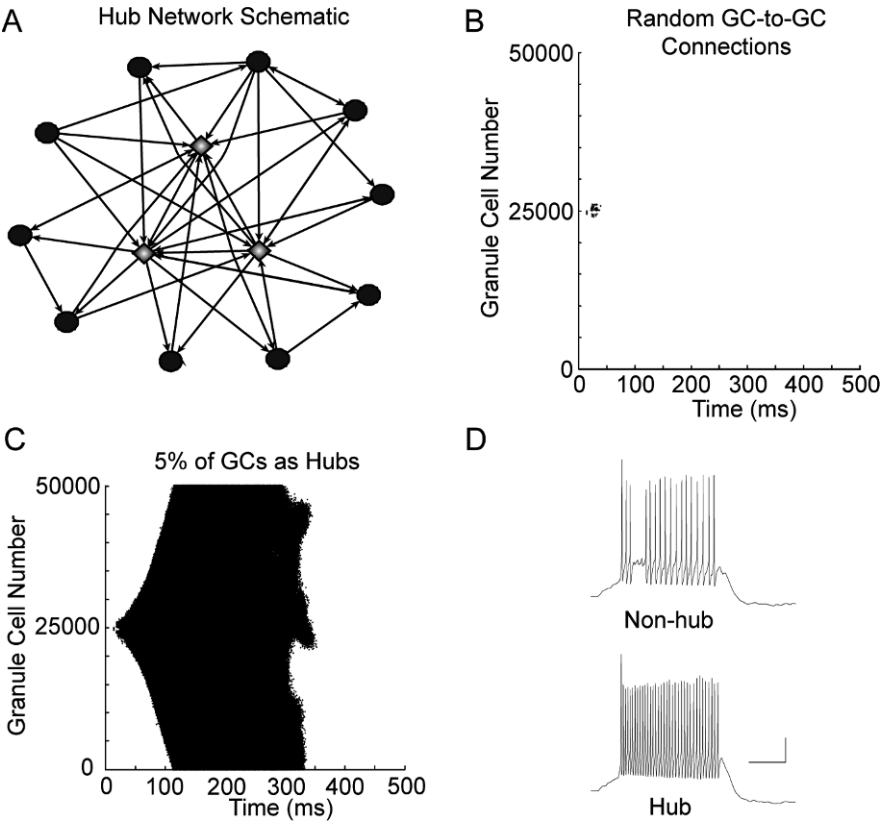

Fig. 5 Granule cell hubs can promote hyperexcitability in the dentate gyrus. **a**. Schematic of a hub network. Average granule cells (*black circles*) have relatively few connections compared to the highly interconnected hubs (*grey diamonds*). **b**. Raster plot of granule cell activity in response to simulated perforant-path stimulation of 1,000 granule cells, 1 mossy cell, and 5 basket cells, in the network in which sprouted mossy fibers connected randomly onto other granule cells. Note that this network was implemented at 50% mossy fiber sprouting and 50% mossy cell and hilar interneuron loss. **c**. Raster plot of granule cell activity in response to the same stimulation as in (**b**), but in the network in which 5% of granule cells participated in many more connections than the average granule cell. (scale: 20 mV and 100 ms). **d**. Representative traces of a non-hub (*top*) and hub (*bottom*) granule cell (scale: 20 mV and 100 ms). Used with permission from Morgan and Soltesz (2008)

Future Directions for the Dentate Model

Both computational power and our knowledge of the inner workings of the dentate gyrus are expanding rapidly. For computational modelers interested in the dentate, this is an ideal situation. While no model can ever fully capture the complete reality of the biological system it attempts to model, it is only by increasing our knowledge of the biology that we can become more confident in models' abilities to make accurate predictions. Likewise, it is by increasing the complexity and detail of models

that we can learn more about what to look for in biological systems. Thus, modelers must look for numerous ways in which to improve a large-scale model like the one discussed in this chapter in order to increase its realism and predictive utility, some of which have been mentioned previously. Most obviously, the size of the model can be expanded to approach the number of cells in the biological dentate. This expansion would allow the most realistic connectivity, without the need for scaling factors or somewhat arbitrary compensations to synaptic weights and connection numbers. Additionally, it would pave the way for construction of bilateral models of the dentate. While this has already been done for the current model, more biological data is required to better implement the commissural connectivity and more computational power is necessary to handle the doubling of the model's size. Further additions to the model that are currently in progress are the inclusion of the omitted interneurons. Specifically, model MOPP cells are nearly completed and will be included in the model soon. Numerous other model expansions have not yet begun but could increase the biological realism of the model as well as present new and interesting questions. These include the addition of short-term and long-term plasticity mechanisms (and the requisite inclusion of NMDA synaptic elements), gap junctions, and realistic dendritic arbors like the axonal distributions in Fig. 3. Finally, the dentate model can be combined with other detailed models of entorhinal cortex, CA1, CA3, and the subiculum to create a truly realistic hippocampal circuit.

Highly detailed, large-scale models of hippocampal microcircuits will someday make it possible to cheaply and efficiently test new therapeutic agents for neurological disorders such as epilepsy, determine the effects of selective surgical lesions on hippocampal function, and provide new insights into the interplay between hippocampus and other brain regions in pathological states (Soltesz and Staley 2008). As computational resources expand and new biological data is discovered, computational modeling will only become more useful as a tool to tie all of our newfound knowledge together and create order from complexity.

Acknowledgments This work was funded by NIH grant NS35915 to IS and UCI MSTP to RM.

Further Reading

Acsady L, Kamondi A, Sik A, Freund T, Buzsaki G (1998) GABAergic cells are the major postsynaptic targets of mossy fibers in the rat hippocampus. J Neurosci 18, 3386–3403.

Acsady L, Katona I, Martinez-Guijarro FJ, Buzsaki G, Freund TF (2000) Unusual target selectivity of perisomatic inhibitory cells in the hilar region of the rat hippocampus. J Neurosci 20, 6907–6919.

Amaral DG (1978) A Golgi study of cell types in the hilar region of the hippocampus in the rat. J Comp Neurol 182, 851–914.

Aradi I and Holmes WR (1999) Role of multiple calcium and calcium-dependent conductances in regulation of hippocampal dentate granule cell excitability. J Comput Neurosci 6, 215–235.

Barabasi AL and Albert R (1999) Emergence of scaling in random networks. Science 286, 509–512.

Bartos M, Vida I, Frotscher M, Geiger JRP, Jonas P (2001) Rapid signaling at inhibitory synapses in a dentate gyrus interneuron network. J Neurosci 21, 2687–2698.

Blasco-Ibanez JM, Martinez-Guijarro FJ, Freund TF (2000) Recurrent mossy fibers preferentially innervate parvalbumin-immunoreactive interneurons in the granule cell layer of the rat dentate gyrus. Neuroreport 11, 3219–3225.

Boss BD, Peterson GM, Cowan WM (1985) On the number of neurons in the dentate gyrus of the rat. Brain Res 338, 144–150.

Buckmaster PS and Dudek FE (1999) In vivo intracellular analysis of granule cell axon reorganization in epileptic rats. J Neurophysiol 81, 712–721.

Buckmaster PS and Jongen-Relo AL (1999) Highly specific neuron loss preserves lateral inhibitory circuits in the dentate gyrus of kainate-induced epileptic rats. J Neurosci 19, 9519–9529.

Buckmaster PS and Schwartzkroin PA (1994) Hippocampal mossy cell function: a speculative view. Hippocampus 4, 393–402.

Buckmaster PS, Strowbridge BW, Kunkel DD, Schmiege DL, Schwartzkroin PA (1992) Mossy cell axonal projections to the dentate gyrus molecular layer in the rat hippocampal slice. Hippocampus 2, 349–362.

Buckmaster PS, Strowbridge BW, Schwartzkroin PA (1993) A comparison of rat hippocampal mossy cells and CA3c pyramidal cells. J Neurophysiol 70, 1281–1299.

Buckmaster PS, Wenzel HJ, Kunkel DD, Schwartzkroin PA (1996) Axon arbors and synaptic connections of hippocampal mossy cells in the rat in vivo. J Comp Neurol 366, 270–292.

Buckmaster PS, Yamawaki R, Zhang GF (2002a) Axon arbors and synaptic connections of a vulnerable population of interneurons in the dentate gyrus in vivo. J Comp Neurol 445, 360–373.

Buckmaster PS, Zhang GF, Yamawaki R (2002b) Axon sprouting in a model of temporal lobe epilepsy creates a predominantly excitatory feedback circuit. J Neurosci 22, 6650–6658.

Chen K, Aradi I, Thon N, Eghbal-Ahmadi M, Baram TZ, Soltesz I (2001) Persistently modified h-channels after complex febrile seizures convert the seizure-induced enhancement of inhibition to hyperexcitability. Nat Med 7, 331–337.

Claiborne BJ, Amaral DG, Cowan WM (1990) Quantitative, three-dimensional analysis of granule cell dendrites in the rat dentate gyrus. J Comp Neurol 302, 206–219.

Cossart R, Dinocourt C, Hirsch JC, Merchan-Perez A, De Felipe J, Ben-Ari Y, Esclapez M, Bernard C (2001) Dendritic but not somatic GABAergic inhibition is decreased in experimental epilepsy. Nat Neurosci 4, 52–62.

Desmond NL and Levy WB (1985) Granule cell dendritic spine density in the rat hippocampus varies with spine shape and location. Neurosci Lett 54, 219–224.

Dyhrfjeld-Johnsen J, Santhakumar V, Morgan RJ, Huerta R, Tsimring L, Soltesz I (2007) Topological determinants of epileptogenesis in large-scale structural and functional models of the dentate gyrus derived from experimental data. J Neurophysiol 97, 1566–1587.

Freund TF and Buzsaki G (1996) Interneurons of the hippocampus. Hippocampus 6, 347–470.

Frotscher M, Seress L, Schwerdtfeger WK, Buhl E (1991) The mossy cells of the fascia dentata: a comparative study of their fine structure and synaptic connections in rodents and primates. J Comp Neurol 312, 145–163.

Gaarskjaer FB (1978) Organization of mossy fiber system of rat studied in extended Hippocampi .1. Terminal area related to number of granule and pyramidal cells. J Comp Neurol 178, 49–71.

Geiger JRP, Lubke J, Roth A, Frotscher M, Jonas P (1997) Submillisecond AMPA receptor-mediated signaling at a principal neuron-interneuron synapse. Neuron 18, 1009–1023.

Gulyas AI, Hajos N, Freund TF (1996) Interneurons containing calretinin are specialized to control other interneurons in the rat hippocampus. J Neurosci 16, 3397–3411.

Gulyas AI, Miettinen R, Jacobowitz DM, Freund TF (1992) Calretinin is present in nonpyramidal cells of the rat hippocampus. 1. A new type of neuron specifically associated with the mossy fiber system. Neuroscience 48, 1–27.

Halasy K and Somogyi P (1993) Subdivisions in the multiple GABAergic innervation of granule cells in the dentate gyrus of the rat hippocampus. Eur J Neurosci 5, 411–429.

Hama K, Arii T, Kosaka T (1994) Three-dimensional organization of neuronal and glial processes: high voltage electron microscopy. Microsci Res Tech 29, 357–367.

Han ZS, Buhl EH, Lorinczi Z, Somogyi P (1993) A high degree of spatial selectivity in the axonal and dendritic domains of physiologically identified local-circuit neurons in the dentate gyrus of the rat hippocampus. Eur J Neurosci 5, 395–410.

Heinemann U, Beck H, Dreier JP, Ficker E, Stabel J, Zhang CL (1992) The dentate gyrus as a regulated gate for the propagation of epileptiform activity. Epilepsy Res Suppl 7, 273–280.

Howard A, Tamas G, Soltesz I (2005) Lighting the chandelier: new vistas for axo-axonic cells. Trends Neurosci 28, 310–316.

Katona I, Acsady L, Freund TF (1999) Postsynaptic targets of somatostatin-immunoreactive interneurons in the rat hippocampus. Neuroscience 88, 37–55.

Kneisler TB and Dingledine R (1995) Spontaneous and synaptic input from granule cells and the perforant path to dentate basket cells in the rat hippocampus. Hippocampus 5, 151–164.

Li XG, Somogyi P, Tepper JM, Buzsaki G (1992) Axonal and dendritic arborization of an intracellularly labeled chandelier cell in the Ca1 region of rat hippocampus. Exp Brain Res 90, 519–525.

Lothman EW, Stringer JL, Bertram EH (1992) The dentate gyrus as a control point for seizures in the hippocampus and beyond. Epilepsy Res Suppl 7, 301–313.

Lubke J, Frotscher M, Spruston N (1998) Specialized electrophysiological properties of anatomically identified neurons in the hilar region of the rat fascia dentata. J Neurophysiol 79, 1518–1534.

Lytton WW, Hellman KM, Sutula TP (1998) Computer models of hippocampal circuit changes of the kindling model of epilepsy. Artif Intell Med 13, 81–97.

Milo R, Shen-Orr S, Itzkovitz S, Kashtan N, Chklovskii D, Alon U (2002) Network motifs: simple building blocks of complex networks. Science 298, 824–827.

Morgan RJ and Soltesz I (2008) Nonrandom connectivity of the epileptic dentate gyrus predicts a major role for neuronal hubs in seizures. Proc Natl Acad Sci U S A 105, 6179–6184.

Nomura T, Fukuda T, Aika Y, Heizmann CW, Emson PC, Kobayashi T, Kosaka T (1997a) Distribution of nonprincipal neurons in the rat hippocampus, with special reference to their dorsoventral difference. Brain Res 751, 64–80.

Nomura T, Fukuda T, Aika Y, Heizmann CW, Emson PC, Kobayashi T, Kosaka T (1997b) Laminar distribution of non-principal neurons in the rat hippocampus, with special reference to their compositional difference among layers. Brain Res 764, 197–204.

Patton PE and Mcnaughton B (1995) Connection matrix of the hippocampal-formation. 1. the Dentate Gyrus. Hippocampus 5, 245–286.

Prill RJ, Iglesias PA, Levchenko A (2005) Dynamic properties of network motifs contribute to biological network organization. PLoS Biol 3, e343.

Rall W, Burke RE, Holmes WR, Jack JJ, Redman SJ, Segev I (1992) Matching dendritic neuron models to experimental data. Physiol Rev 72, S159–186.

Reigl M, Alon U, Chklovskii DB (2004) Search for computational modules in the *C. elegans* brain. BMC Biol 2, 25.

Ribak CE, Seress L, Amaral DG (1985) The development, ultrastructure and synaptic connections of the mossy cells of the Dentate Gyrus. J Neurocytol 14, 835–857.

Santhakumar V, Aradi I, Soltesz I (2005) Role of mossy fiber sprouting and mossy cell loss in hyperexcitability: a network model of the dentate gyrus incorporating cell types and axonal topography. J Neurophysiol 93, 437–453.

Santhakumar V, Bender R, Frotscher M, Ross ST, Hollrigel GS, Toth Z, Soltesz I (2000) Granule cell hyperexcitability in the early post-traumatic rat dentate gyrus: the 'irritable mossy cell' hypothesis. J Physiol 524 Pt 1, 117–134.

Scharfman HE (1991) Dentate hilar cells with dendrites in the molecular layer have lower thresholds for synaptic activation by perforant path than granule cells. J Neurosci 11, 1660–1673.

Sik A, Penttonen M, Buzsaki G (1997) Interneurons in the hippocampal dentate gyrus: an in vivo intracellular study. Eur J Neurosci 9, 573–588.

Soltesz I and Staley KJ (2008) Computational Neuroscience in Epilepsy. Elsevier, New York.
Song S, Sjostrom PJ, Reigl M, Nelson S, Chklovskii DB (2005) Highly nonrandom features of synaptic connectivity in local cortical circuits. PLoS Biol 3, e68.
Soriano E, Nitsch R, Frotscher M (1990) Axo-axonic chandelier cells in the rat fascia dentata: Golgi-electron microscopy and immunocytochemical studies. J Comp Neurol 293, 1–25.
Sporns O and Kotter R (2004) Motifs in brain networks. PLoS Biol 2, e369.
Staley KJ, Otis TS, Mody I (1992) Membrane properties of dentate gyrus granule cells: comparison of sharp microelectrode and whole-cell recordings. J Neurophysiol 67, 1346–1358.
Walter C, Murphy BL, Pun RY, Spieles-Engemann AL, Danzer SC (2007) Pilocarpine-induced seizures cause selective time-dependent changes to adult-generated hippocampal dentate granule cells. J Neurosci 27, 7541–7552.
Watts DJ and Strogatz SH (1998) Collective dynamics of 'small-world' networks. Nature 393, 440–442.
Wenzel HJ, Buckmaster PS, Anderson NL, Wenzel ME, Schwartzkroin PA (1997) Ultrastructural localization of neurotransmitter immunoreactivity in mossy cell axons and their synaptic targets in the rat dentate gyrus. Hippocampus 7, 559–570.
West MJ (1990) Stereological studies of the hippocampus – a comparison of the hippocampal subdivisions of diverse species including Hedgehogs, Laboratory Rodents, wild mice and men. Progr Brain Res 83, 13–36.
West MJ, Danscher G, Gydesen H (1978) A determination of the volumes of the layers of the rat hippocampal region. Cell Tissue Res 188, 345–359.
Yoshimura Y and Callaway EM (2005) Fine-scale specificity of cortical networks depends on inhibitory cell type and connectivity. Nat Neurosci 8, 1552–1559.